THE JOURNAL OF PHYSICAL CHEMISTRY Letters

pubs.acs.org/JPCL Letter

First-Order Phase Transition in Liquid Ag to the Heterogeneous G-Phase

Qi An,* William L. Johnson,* Konrad Samwer, Sydney L. Corona, and William A. Goddard, III*

Cite This: J. Phys. Chem. Lett. 2020, 11, 632−645 Read Online

ACCESS | Metrics & More | Article Recommendations | Supporting Information

ABSTRACT: A molten metal is an atomic liquid that lacks directional bonding and is free from chemical ordering effects. Experimentally, liquid metals can be undercooled by up to ∼20% of their melting temperature but crystallize rapidly in subnanosecond time scales at deeper undercooling. To address this limited metastability with respect to crystallization, we employed molecular dynamics simulations to study the thermodynamics and kinetics of the glass transition and crystallization in deeply undercooled liquid Ag. We present direct evidence that undercooled liquid Ag undergoes a first-order configurational freezing transition from the high-temperature homogeneous disordered liquid phase (L) to a metastable, heterogeneous, configurationally ordered state that displays elastic rigidity with a persistent and finite shear modulus, μ. We designate this ordered state as the G-phase and conclude it is a metastable non-crystalline phase. We show that the L−G transition occurs by nucleation of the G-phase from the L-phase. Both the L- and G-phases are metastable because both ultimately crystallize. The observed first-order transition is reversible: the G-phase displays a first-order melting transition to the L-phase at a coexistence temperature, $T_{G,M}$. We develop a thermodynamic description of the two phases and their coexistence boundary.

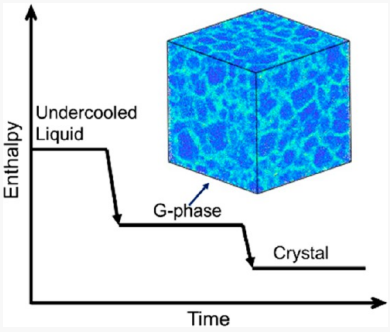

Since the early work of Goldstein,[1] the picture that has formed the basis for the thermodynamic description of deeply undercooled liquids and their freezing transition to the glassy state is as follows.[2−6] An undercooled liquid that configurationally freezes to a glass is a metastable state of matter that ultimately crystallizes given adequate time to explore its entire available configurational phase space. Crystallization is triggered by a relatively improbable fluctuation whereby the liquid or glass crosses a crystal nucleation barrier. If the waiting time for this improbable fluctuation sufficiently exceeds the time required for the liquid to explore its available noncrystalline configurations, one may define a metastable configurational entropy for the liquid, $S_C = \ln W_C$, where W_C enumerates the available noncrystalline configurations or inherent states versus their total potential energy (PE), ϕ.

The laboratory glass transition is most commonly viewed as a dynamic transition accompanied by a dramatic slow-down in kinetics as one approaches the glass transition temperature, T_g. The possible existence of an underlying thermodynamic glass transition is at best a controversial topic. Notwithstanding, there are numerous reports in the literature suggesting that a metastable undercooled liquid may exist in multiple thermodynamic phases separated by so-called liquid−liquid phase transitions (LLPTs) at coexistence boundaries. Most reported examples involve either complex molecular liquids such as H_2O,[7] D-mannitol,[8] triphenyl phosphite,[9] or elemental liquids such as Si, where an LLPT transition is believed to be related to the crossover from a covalent tetrahedrally coordinated liquid state to metallically bonded state with higher atomic coordination,[10] or elemental P and S, which can form molecular or extended structures.[11,12] For metals, evidence of an LLPT has been reported in complex multicomponent bulk metallic glass-forming alloys.[13−15] Particularly in the case of metallic glass-forming alloys, the reported LLPTs may be more appropriately viewed as thermodynamic liquid−glass phase transitions. Experimental studies of LLPTs are frequently hampered by the limited metastability of undercooled melts due to intervening crystallization. Even so, deeply undercooled metallic liquids can be achieved experimentally,[16] especially with the electromagnetic levitation technique.[17−19]

We consider here a single-component metallic liquid, which is the simplest atomic liquid with neither directional bonding nor chemical ordering effects. In addition, elemental metal liquids are expected to be rheologically very fragile.[20] Elemental amorphous metals were first produced experimentally by deposition of metal vapor onto cryogenically cooled substrates held at 4.2 K, where atomic mobility and crystallization are kinetically arrested.[21] While the as-deposited thin films were shown by diffraction methods to be amorphous, they subsequently crystallized abruptly upon heating to ∼30−50 K,

Received: December 13, 2019
Accepted: January 4, 2020
Published: January 4, 2020

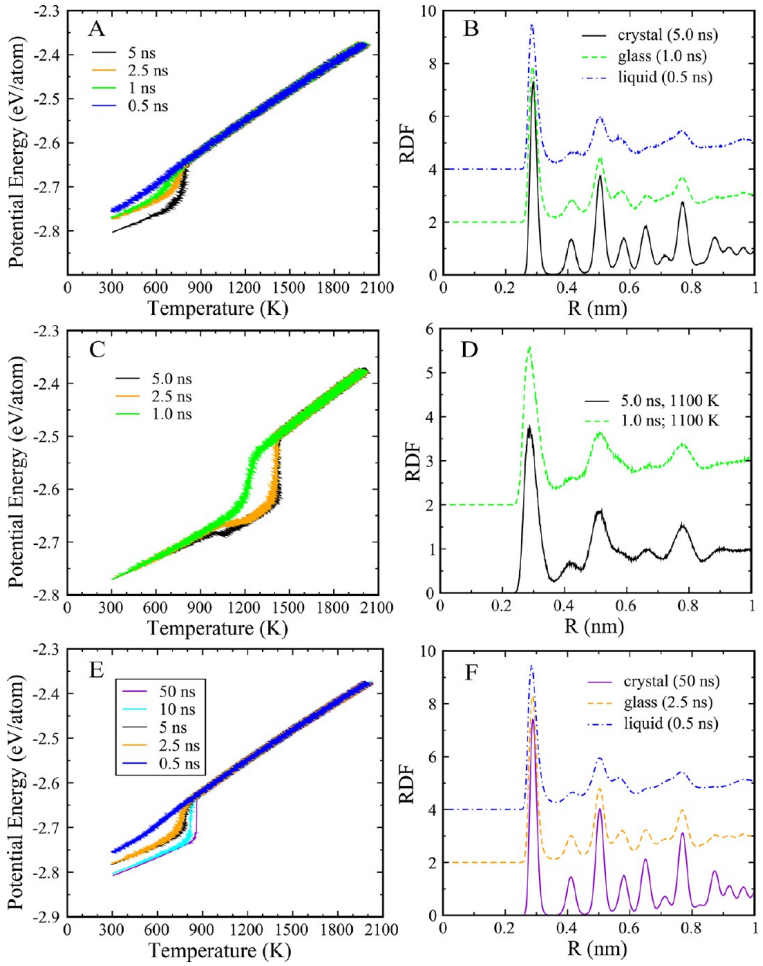

Figure 1. Cooling and heating process of Ag: (A) cooling process for the 32 000 atom system with various cooling rates of 3.4×10^{12}, 1.7×10^{12}, 0.68×10^{12}, and 0.34×10^{12} K/s; (B) RDF of the quenched structure at 300 K with various cooling rates of 3.4×10^{12}, 1.7×10^{12}, and 0.34×10^{12} K/s; (C) heating of glassy Ag (32 000 atoms) with various heating rates of 1.7×10^{12}, 0.68×10^{12}, and 0.34×10^{12} K/s; (D) RDF of heated structures at 1100 K; (E) cooling of the 256 000 atom system with various cooling rates of 3.4×10^{12}, 0.68×10^{12}, 0.34×10^{12}, 1.7×10^{11}, and 0.34×10^{11} K/s; and (F) RDF of the quenched structure at 300 K with various cooling rates of 3.4×10^{12}, 0.68×10^{12}, and 0.34×10^{11} K/s.

suggesting that an elemental amorphous metal is inherently unstable with respect to crystal nucleation and/or growth. The crystal growth velocity in undercooled liquids was later determined in both theory and experiment.[17,22] On the basis of the low crystallization temperature, it was also assumed that an elemental metallic glass must exhibit a very low glass transition temperature, T_g. More recently, it was reported that picosecond laser pulse melting of submicron strips of refractory metals (Ta and V) followed by quenching at a rate exceeding 10^{12} K/s produces a glass in the melted zone[23] that remains stable at ambient temperature. Using molecular dynamics (MD) simulations, An et al.[24] demonstrated that 30 nm liquid Cu nanodroplets quenched from the equilibrium melt form a glass at cooling rates as low as 2×10^{12} K/s when quenched onto a low-temperature noncrystalline metal substrate. A broad apparent glass transition was observed during quenching at around 700−800 K, evidenced by a drop in liquid enthalpy and freezing of the atomic configuration. By contrast, quenching the same nanodroplet onto a cold crystalline Cu substrate resulted in the droplet crystallizing by crystal growth from the substrate. It was concluded that the quench rate was sufficient to suppress crystal nucleation within the droplet but insufficient to prevent crystal growth from the crystalline substrate.

In the present work, we carried out continuous MD cooling simulations to study glass formation upon quenching of pure liquid Ag. We found that cooling rates as low as $\sim 3.4 \times 10^{11}$ K/s are sufficient to form a glass by quenching from the liquid. Indeed, undercooled states of liquid Ag can be achieved experimentally using even lower cooling rates.[25] We found that the enthalpy drop during cooling through the glass transition becomes progressively sharper and larger as the cooling rate is lowered. These observations motivated us to study of the thermodynamics and kinetics of the glass transition and crystal nucleation for isothermal (N,P,T) and (N,V,T) ensembles. For isothermal ensembles, the liquid to glass transition for elemental Ag develops the hallmark signatures of a first-order thermodynamic phase transition, including latent heat, entropy jump, reversibility (remelting of the glass), and cooling/heating hysteresis, plus evidence that the glass phase forms by nucleation from the liquid (L) phase. We developed a method to image the

https://dx.doi.org/10.1021/acs.jpclett.9b03699
J. Phys. Chem. Lett. 2020, 11, 632−645

spatial distribution of configurational enthalpy and entropy to show that this metastable glassy state, denoted as the G-phase, is inherently heterogeneous with a characteristic length scale, Λ. Using two-phase coexistence simulations, we demonstrate that the transition from undercooled liquid L-phase to the G-phase is reversible. We show that the L- and G-phases coexist in metastable equilibrium at a glass melting temperature $T_{G,M}$. We locate $T_{G,M}$ by observing the motion of the L−G interface above and below the coexistence temperature. Unlike the more fluid L-phase, the G-phase exhibits persistent long-range elastic rigidity with a finite shear modulus, $\mu(T)$, that persists over the time scale of its metastability, as determined by ultimate crystal nucleation. That is, atomic displacements in the metastable G-phase obey elastic compatibility constraints (i.e., Saint Venant equations)[26] that restrict atomic rearrangement in the glass by imposing persistent long-range correlations in the atomic configuration. These correlations extend over distances well beyond the range of interatomic forces. We propose that the discontinuous emergence of persistent long-range elastic interactions is the underlying mechanism that results in a first-order L−G transition and accompanying reduction in configurational entropy. The present results demonstrate that the heterogeneous elemental Ag G-phase, like the gas and liquid phases, is a macroscopically isotropic, albeit metastable, state.

To explore the thermodynamics and kinetics of undercooled elemental Ag, we carried out MD simulations over time scales ranging up to tens of nanoseconds on systems with sizes varying at N = 4000, 32 000 and 256 000 atoms. Briefly, we use the Ag Embedded Atom Model (EAM)[27] with the parameters fitted to quantum mechanics (QM) simulations and experiment with the MD controlled by the LAMMPS software.[28] The simulation details can be found in the Supporting Information (SI).

Figure 1A shows the PE per atom, $\phi(T)$, of a 32 000 atom Ag system versus temperature under constant cooling/heating rate conditions between 300 and 2000 K, a temperature range of ΔT = 1700 K, with 0.5, 1.0, 2.5, and 5.0 ns cooling times. For the highest cooling rate (3.4×10^{12} K/s; blue curve), we observe an inflection in the $\phi(T)$ cooling curve at around 600−700 K. While vibrational modes rapidly equilibrate during the quench, configurational relaxation is suppressed by the ultrafast cooling, and the system exhibits only weak evidence of configurational freezing. No evidence of crystallization is observed, as confirmed by the liquid-like pair correlation function obtained in Figure 1B following the quench. At the lowest cooling rate (3.4×10^{11} K/s; black curve), a factor of 10 lower, crystallization intervenes sharply at ∼750 K, as evidenced by the pair correlation function in Figure 1B. Further analysis shows that the crystallized sample exhibits a face-centered cubic (fcc) structure in which a single crystal spans the entire MD cell.

For intermediate cooling rates, glass formation occurs at both 1.7×10^{12} K/s (green curve) and a still lower cooling rate of 6.8×10^{11} K/s (orange curve). For the two intermediate cooling rates, the system displays rather abrupt configurational freezing with a sharp inflection at ∼700 K and a final PE intermediate between the crystallized system and the most rapidly quenched system. The pair correlation function of the latter system reveals that it is glassy (Figure 1B). Henceforth, we shall discriminate between liquid (L), glass (G), and crystal (X) phases. As a preliminary structural fingerprint for crystallinity, the intensity of the second peak in the radial distribution function (RDF) (Figure 1B) around 0.4 nm provides a useful signature. A more detailed analysis of the glass structure will be given below, revealing that there is no long-range order in the G structures. The second RDF peak represents the distance between atoms at opposite vertices of an octahedron. Octahedral atomic clusters are largely absent in metallic glasses but are present in the ratio of 1 per atom in a fcc crystal. Finally, we note that the apparent T_g of the green and orange curves lies slightly below the crystallization event T_x (black curve).

Figure 1C displays reheating curves obtained for the glass produced by quenching at 1.7×10^{12} K/s (green curve in Figure 1A). The reheating rates are 1.7×10^{12}, 6.8×10^{11}, and 3.4×10^{11} K/s. At the highest heat rate (green curve), the glass $\phi_G(T)$ curve shows only a vibrational Dulong−Petit term $[(3/2)RT]$ plus a small anharmonic "aT^2" term up to a temperature of ∼1200 K. The glass then "remelts" directly back to the liquid with no apparent intervening crystallization. At the two lower heating rates, the glass crystallizes upon heating with a sharp drop in $\phi(T)$ at ∼1000 K (black curve at 3.4×10^{11} K/s) and ∼1150 K (orange curve at 6.8×10^{11} K/s). Continued heating results in the crystallized samples remelting at about 1400−1450 K. Two-phase single crystal−liquid simulations described below show that the equilibrium melting point of our model fcc Ag is 1250 K (see Figure S1A,B, SI). Thus, some overheating of the crystalline Ag is observed at these heating rates. We characterize the liquid−glass versus a crystal using the second peak in the RDF, as shown in Figure 1B,D. Even at the ultrafast heating rates used in Figure 1C, the direct "remelting" of the glass is extremely sharp. The apparent slope of the $\phi(T)$ curve during remelting is equivalent to a specific heat jump of about $\Delta c_p \approx 120$ J/mol·K $\approx 15R$ for the crystal and $\Delta c_p \approx 85$ J/mol·K $\approx 10R$ for the glass, respectively. Such a sharp remelting transition points to first-order melting. There is clear asymmetry between the critical cooling rate versus heating rate required to avoid crystallization. Figure 1C shows that the minimum heating rate to bypass crystallization upon reheating the glass is greater than 1.7×10^{12} K/s (T glass to liquid ≈ 1200 K, green curve Figure 1C), while the minimum cooling rate to form glass upon cooling is less than 6.8×10^{11} K/s (T liquid to glass ≈ 750 K, orange curve Figure 1A). A similar heating vs cooling asymmetry is actually observed experimentally in bulk metallic glasses.[29]

To investigate system size effects on the glass transition and crystallization kinetics, we carried out additional simulations for a larger system with doubled MD cell parameters (16 versus 8 nm) and N = 256 000 atoms. Results for the constant cooling simulation for the larger system are shown in Figure 1E,F. Figure 1E shows the PE per atom obtained at various quench rates. Figure 1F shows the corresponding RDF obtained following quenching at rates of 1.7×10^{12}, 0.68×10^{12}, and 0.34×10^{11} K/s. We observe that the critical quench rate to form the glass appears to be lower than that observed for the N = 32 000 atom system. At first, this result seems puzzling when one considers that traditional homogeneous nucleation theory predicts that the crystal nucleation rate should be related to system size.[30] Comparing Figure 1A,B with Figure 1E,F implies that the waiting time for crystal nucleation increases with cell size, which suggests that the periodic boundary conditions imposed in our simulations influenced the formation of a critical crystal nucleus for the 32 000 atom system. However, the 16 nm cell of the 256 000 atom system was sufficiently large that only the G-phase was formed. In the following, we investigate this behavior and show that periodic boundary conditions are the underlying origin of this system size effect. The solidification and nucleation kinetics of metallic liquids could be examined experimentally using the fine (10−20 pm) droplet samples.[31]

https://dx.doi.org/10.1021/acs.jpclett.9b03699
J. Phys. Chem. Lett. 2020, 11, 632−645

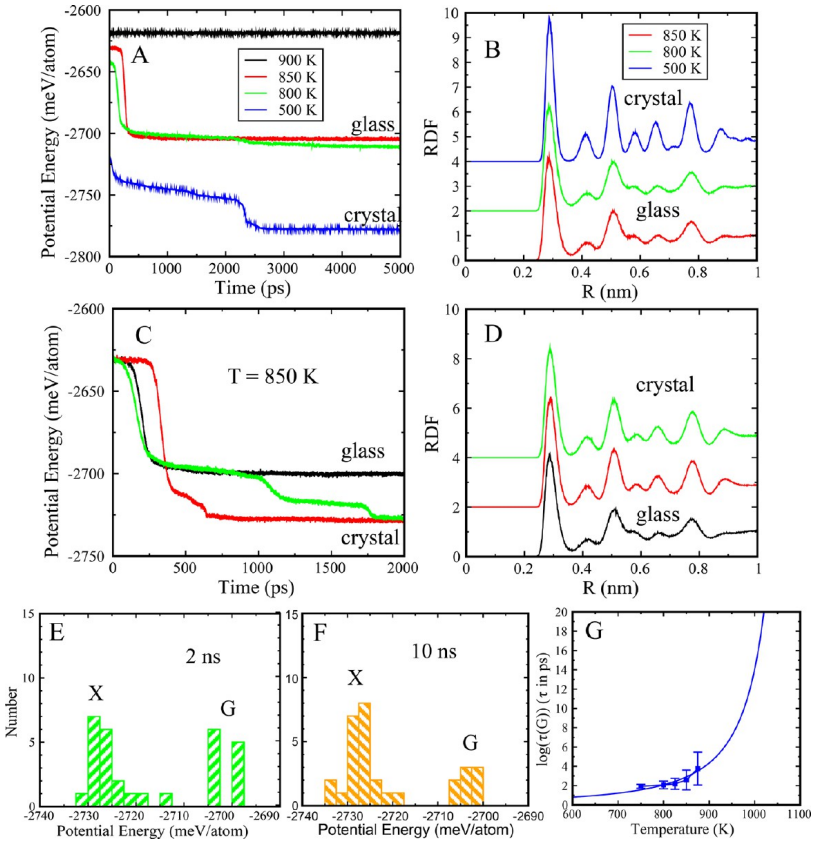

Figure 2. (A) Isothermal MD for a 32 000 atom system at 900 (black), 850 (red), 800 (green), and 500 K (blue) and (B) with RDFs from 850, 800, and 500 K. (C) Isotherms at 850 K: Run 1 (black), 2 (red), 3 (green). (D) RDFs for various runs, leading to an either glass or crystal phase. (E,F) PE histogram of X- and G-phases at 2 and 10 ns at T = 800 K. (G) Time−temperature−transformation (t−T−T diagram) for glass nucleation from the liquid.

To further identify this G-phase, we extended the RDF analysis to 2.0 nm for the quenched crystal phase. The RDFs for the L-phase at 1300 K (above T_m) and 300 K and for the G-phase at 300 and 0 K are shown in Figure S2A, SI. The structure factor $S(q)$ for these three phases was computed and is displayed in Figure S2B. The G-phase exhibits a structural character similar to that of the L-phase. The long-range order exhibited by the crystal phase disappears beyond 1.2 nm in the G-phase, showing that it is *not* a crystal phase.

To illustrate the structural difference between the G-phase and L-phase, we performed Honeycutt−Anderson (HA) analysis[32] on these two phases at 800 K. As shown in Table S1, SI, the characteristic HA indices of the G-phase are mainly 1421 and 1422, suggesting large amounts of fcc and hcp character in the G-phase. In contrast, the characteristic HA indices in the L-phase are 1541 and 1551, indicating that the liquid structure has significant icosahedral character. Experimental evidence of the icosahedral short-range order was obtained in other undercooled elemental metallic liquids, e.g., Ni, Zr, Fe, and Co.[18,19] We also performed HA analysis on the larger G-phase with 256 000 atoms/cell. The results, listed in Table S1, show that the 1421 and 1422 HA indices increase slightly as the system size increases from 32 000 to 256 000 atoms. Thus, this character of the G-phase is expected to apply to the infinite system.

The ultrafast rates used in constant heating and cooling runs discussed above bias the system toward falling out of equilibrium with respect to configurational degrees of freedom. At these rates, the application of equilibrium thermodynamic principles to study glass formation is questionable at best. To establish metastable configurational equilibrium in a liquid and/or glass at fixed temperature requires configurational relaxation of the liquid/glass for times significantly longer than the liquid α-relaxation time. Crystallization inevitably intervenes. To explore metastable liquid/glass equilibration and the limits of metastability imposed by crystal nucleation, we carried out isothermal simulations vs time. This was implemented by taking snapshots from the MD configurations during a constant cooling run at a target temperature T and then imposing a MD thermostat to fix and hold the temperature. This allowed the liquid configuration (blue curve in Figure 1A) to evolve at the fixed temperature. Configurational evolution of the liquid then proceeds at the given temperature until interrupted by glass formation and/or crystal nucleation.

Figure 2A shows $\phi(T)$ vs time for these isothermal segments for the 32 000 atom system. At T = 900 K, the liquid is equilibrated within the first few picoseconds displaying a fixed $\phi_L(T)$ that remains constant (with fluctuations about its average value) out to 5 ns. There is no evidence of either crystallization or configurational freezing at 900 K. The liquid achieves metastable equilibrium with respect to both vibrations and

https://dx.doi.org/10.1021/acs.jpclett.9b03699
J. Phys. Chem. Lett. 2020, 11, 632−645

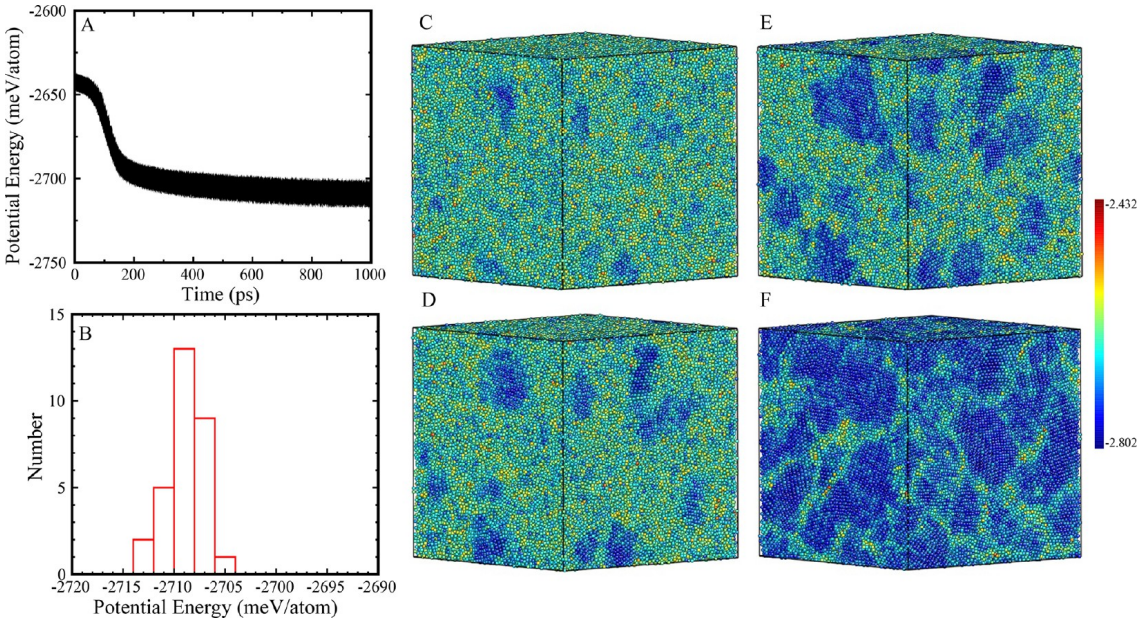

Figure 3. (A) Thirty isothermal runs for a 256 000 atom system at 800 K; (B) histogram of the PE of G-phases at 1 ns at $T = 800$ K; (C–F) PE density map for one glass structure at various times: (C) 50 ps, (D) 75 ps, (E) 100 ps, and (F) 1 ns (color coded by PE density).

configurations. The simulations at 850 and 800 K show an equilibrated liquid that abruptly undergoes a transition to a glass state following a waiting time that varies from 100 to 300 ps. Prior to this glass formation event, the liquid $\phi_L(T)$ remains constant, showing only fluctuations about its metastable equilibrium value. Once nucleated, the glass state rapidly equilibrates to a constant and well-defined value of $\phi_G(T)$ that subsequently persists for the duration of the simulation (5 ns). At 500 K, a glass forms initially and then exhibits a value of $\phi(T)$ that decays steadily and abruptly drops upon crystallization. The RDF analyses of 5 ns structures at 850, 800, and 500 K are displayed in Figure 2B, indicating the liquid to glass/crystal transition. Multiple (30) simulations were carried out at each temperature (Figure S3A–E, SI). Figure 2C shows three representative examples at 850 K. The first example (black curve) results in formation of a stable glass state that persists to 2 ns, yielding a final value of $\phi_G(T) \approx -2705$ meV/atom. In the second example (green curve), the system forms an intermediate glass state with roughly the same PE and then abruptly crystallizes in a two-stage sequence beginning at about 1 ns and followed by a secondary step at 1.75 ns, yielding a final energy $\phi_X(T) \approx -2727$ meV/atom. In the third example (red curve), no intermediate glass is apparent, and crystallization occurs at about 350 ps followed by a secondary step leading to a final $\phi_X(T) \approx -2728$ meV/atom. Figure 2D shows the RDF for the final glass state and crystalline states at 850 K. The relatively smaller value of the second maximum in the glass (or liquid) indicates substantially fewer octahedral atomic clusters versus the fcc crystalline phase.

Of the 30 simulations for $N = 32\,000$, with a duration of 2 ns at 850 K, 11 resulted in formation of a metastable glass, while 19 resulted in a crystallized final state. Thus, the phase evolution pathway in our simulations at 850 K is clearly stochastic. The system selects different pathways depending on the details of the initial MD microstate. Extending the simulations to 10 ns revealed that three of the glasses at 2 ns crystallized while eight persisted to 20 ns without crystallization. It is of interest to examine how the final system PE is distributed after 2 ns or longer simulation times. This is displayed in the histogram in Figure 2E,F. The outcome at 2 ns is clearly bimodal with 11 glass states and 19 crystallized states separated in PE by an apparent gap. After extending the runs from 2 to 10 ns, 3 of the 11 glass states at 2 ns subsequently crystallized. In particular, states of intermediate PE $\phi(T)$ lying in the gap region between glass and crystal energies are apparently relatively unstable, quickly decaying to a lower-energy crystalline state. As glass states crystallize over extended simulation time, their population in the glass peak of the bimodal distribution decays, as seen in Figure 2F. This provides an estimate of the characteristic waiting time for a metastable glass state to crystallize, i.e., the nucleation time for a stable crystal to form and grow in a glass. On the basis of the limited statistics (11 glass states at 2 ns decay to 8 at 10 ns), we estimate a mean crystal nucleation time from a relatively relaxed glass at 2 ns to be ~30 ns.

We carried out ~30 separate MD runs at $T = 750$, 800, 825, 850, and 875 K in the liquid (Figure S3A–E). Using these results, we computed the average elapsed time to the onset of glass nucleation from the liquid at each T. Figure 2G shows the logarithm of the average nucleation time for glass formation vs T. Assuming that the L–G transition is a first-order nucleated process, the plot may be interpreted as a time–temperature–transformation t–T–T diagram for glass nucleation from the liquid. Apparently, for temperatures above 900 K, the glass nucleation time exceeds practical MD simulation capabilities. This is consistent with Figure 2A where the liquid remains metastable throughout the simulation. The solid curve in Figure 2G is a fit to the data based on a simple classical nucleation model for glass nucleation. The fit assumes the nucleation barrier height scales as $(T_{G,M} - T)^{-2}$, where $T_{G,M}$ refers to the thermodynamic melting point of the Ag glass phase. As will be shown below, we determined $T_{G,M}$ to be ~1125 K by using the two-phase simulation method. Therefore, Figure 2G provides

https://dx.doi.org/10.1021/acs.jpclett.9b03699
J. Phys. Chem. Lett. 2020, 11, 632–645

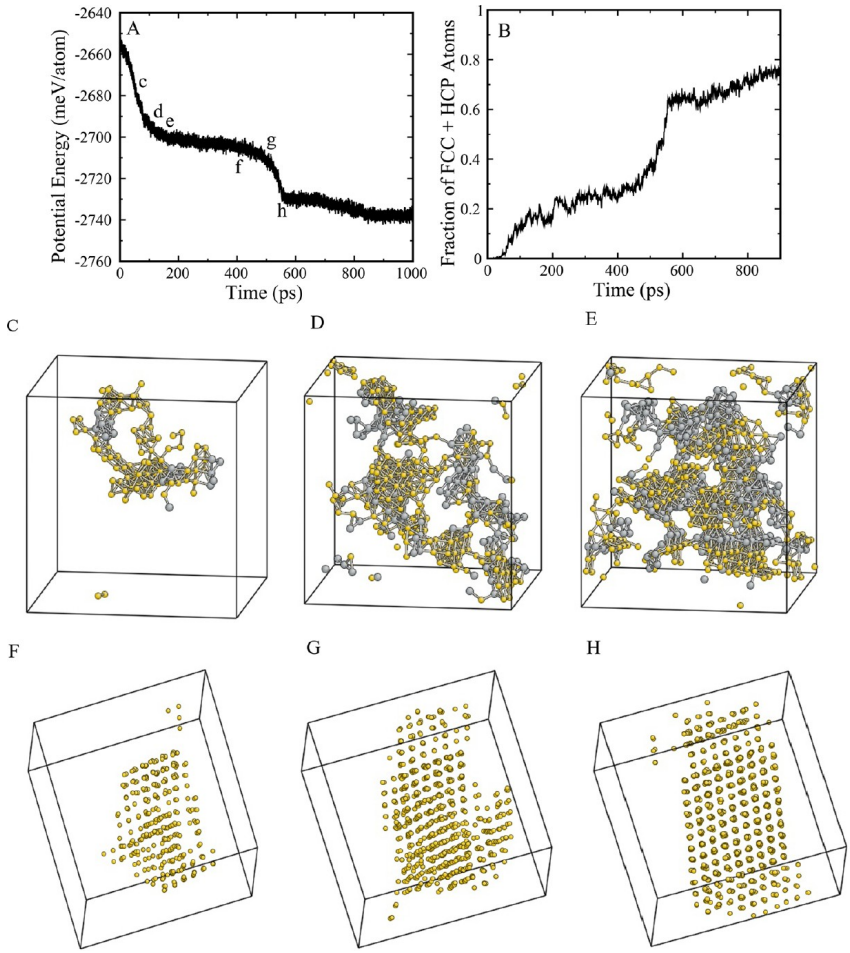

Figure 4. Glass formation and crystallization versus time at 800 K for a 4000 atom system exhibiting the PE versus time, shown in (A). Fraction of fcc + hcp atoms versus time (B). The actual fcc (yellow) and hcp (gray) atoms were identified from the HA analysis as a function of time at 80 (C), 110 (D), and 150 ps (E). We find that distinct and separate clusters of fcc/hcp atoms are formed in local but separate regions. The clusters do not span the MD cell and have a typical radius of ∼2 nm. Crystallization is trigged when a large cluster of fcc atoms forms by merging of fcc grains (F, 400 ps) that merge (G, 500 ps) and ultimately span the MD cell (H, 560 ps). This is followed by rapid formation of a single crystal that includes over 80% of the 4000 atom system, as seen in (B).

direct evidence that the L−G transition occurs by nucleation of the G-phase from the L-phase. It further implies the glass nucleation time above 900 K rises with an $\exp[-C/(T_{G,M} - T)^{-2}]$ dependence. Extrapolation to $T \approx 1000$ K implies a laboratory nucleation time scale of ∼1 s or more.

Following the results shown in Figure 1E,F, we proceeded to assess the effect of the MD cell size on glass nucleation and crystallization during isothermal runs using the larger cell size (16 vs 8 nm) with N = 256 000 atoms. We carried out 30 isothermal runs at 800 K following the same procedures as those for the 32 000 atom system. The PE versus time curves are shown in Figure 3A, and the PE distribution is displayed in Figure 3B. The glass nucleation process can be observed in Figure 3C−F. For the larger system, the L−G transition is observed in every run with no crystallization in any of the runs. Further, the nucleation time for the G-phase is much better defined and repeatable. At 800 K, the mean time for glass nucleation is ∼0.1 ns. Apparently, crystal nucleation is dramatically suppressed in the larger system. This result is quite striking because traditional homogeneous nucleation theory suggests that the waiting time for an initial nucleation event should scale inversely with system size. This size effect is dramatic in that no crystallization occurs in the larger system. To understand the origin of this effect, we examined the mechanism of crystallization in smaller 32 000 and 4000 atom systems using HA analysis to identify how the critical crystal nucleus is formed.

Figure 4A displays the time evolution of the PE during a typical isothermal run for a small 4000 atom system at 750 K. The initial liquid transforms to a glass beginning at ∼50 ps and finishing at ∼120 ps. The glass remains stable to ∼400 ps and then abruptly crystallizes between ∼450 and 550 ps. Using HA analysis, we identified atoms having either an fcc or hcp environment and treated all other atoms as noncrystalline. Figure 4B shows the number of fcc/hcp atoms (essentially close-packed atoms) versus time. During glass formation from the liquid, this number increases to ∼1000 atoms, or ∼25% of 4000 atoms, and then remains roughly constant. Upon crystallization, the number of fcc/hcp atoms jumps abruptly to about 2500

https://dx.doi.org/10.1021/acs.jpclett.9b03699
J. Phys. Chem. Lett. 2020, 11, 632−645

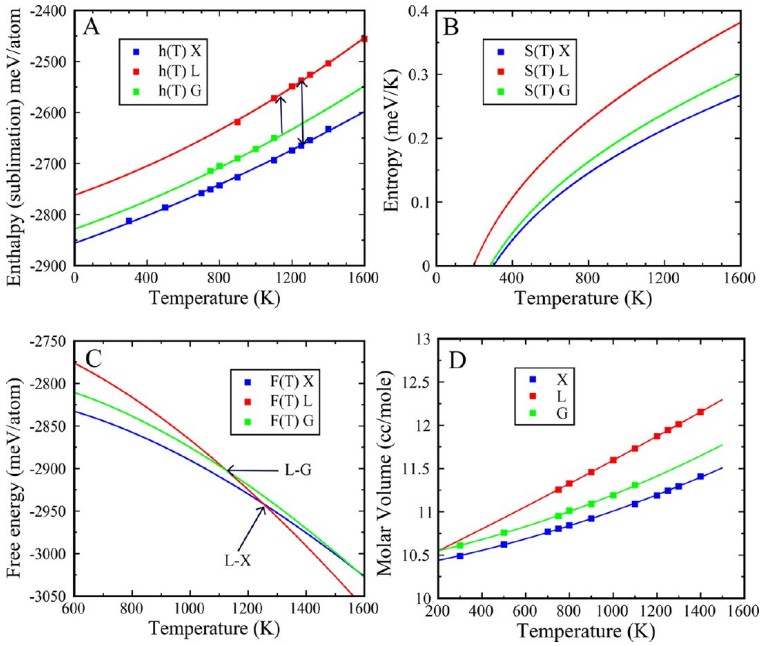

Figure 5. (A) Enthalpy map of various phases (explained in the text) as extracted from our MD simulation of Ag. (B,C) Thermodynamic functions $s(T)$ and $g(T)$ of the liquid, glass, and crystalline phases calculated from the fits to the enthalpy vs T for each phase as described in the text: (B) entropy, (C) free energy (Gibb's at fixed $P = 0$). (D) Molar volume vs T.

atoms (~65% of the atoms) and then continues to steadily increase. Figure 4C–E shows snapshots of all fcc/hcp atoms at 80, 110, and 150 ps as the liquid to glass transition occurs. These atoms form isolated and compact clusters that are separated by a boundary of noncrystalline atoms. The typical radius of these clusters is 1.0–1.5 nm. These clusters contain both fcc and hcp atoms, indicating that the local close-packed structure includes stacking faults. The local clusters are surrounded by regions containing only noncrystalline atoms that comprise the majority of the glass structure. Figure 4F–H shows snapshots illustrating the development of the largest fcc cluster during crystallization. Two ordered clusters transiently merge at about 400 ps, forming a single larger cluster at ~500 ps. This larger cluster impinges on the (upper/lower) boundary of the MD cell, causing this critical cluster to span the MD cell. Owing to the periodic boundary conditions, this cluster interacts with its image on the opposite cell face to form the spanning cluster. At this point, the cluster rapidly grows to fill the entire MD cell.

Thus, we expected that the probability of crystallization of the larger 256,000 atom system (with a ~16 nm cell dimension) would be dramatically reduced. Indeed, none of our 30 cases crystallized. One might expect the probability of a spanning cluster to decrease exponentially, as $e^{-kL/\Lambda}$, with system dimension L, where k is some constant of order unity (based on the present results). We conclude that in the limit $N \rightarrow \infty$ crystallization of the G-phase should become rare and effectively unobservable on the MD time scale. In other words, the metastability of the G-phase with respect to crystallization is quite robust in the thermodynamic limit.

The PE per atom for the various isothermal MD runs shown in Figures 2A,C and 3A is the sum of vibrational and configurational terms. Assuming metastable equilibrium at each T, the average vibrational PE per atom is expected to have the form $\phi^{v}(T) = (3/2)RT + aT^2 + ...$, where the first term is the classic Dulong–Petit contribution and the second (+ higher order) smaller term accounts for anharmonicity (terms beyond second order in T are neglected). Vibrational equilibrium for any phase is achieved rapidly, within ~1 ps, because the system explores the vibrational degrees of freedom at typical Debye frequencies. For a given phase χ, where χ = L, G, or X, assumed to be in equilibrium or metastable equilibrium, we designate its configurational PE at fixed T and $P = 0$ as $\phi^{C}{}_{\chi}(T)$. This is the average configurational PE of the inherent states of the phase χ at T and ambient pressure. In equilibrium, the total average PE is

$$\phi_{\chi}(T) = \phi^{C}{}_{\chi}(T) + (3/2)RT + a_{\chi}T^2 + \text{higher-order anharmonic terms} \quad (1)$$

In general, the anharmonic coefficient a_{χ} depends on the phase because configurational states of higher PE are expected to exhibit greater anharmonicity. In equilibrium or metastable equilibrium of phase χ at T and $P = 0$, the total energy (potential + kinetic energy) is identified directly with the total specific enthalpy $\phi_{\chi}(T) = h_{X}(T, P = 0)$ of phase χ. In equilibrium, enthalpy is a state function of T for each metastable or stable phase. For example, the initial liquid at 900 K (Figure2A) rapidly equilibrates (<1 ps), achieving a stationery value $\phi_{L}(900\ K)$ out to 5 ns. Similarly, at 800 and 850 K (red and green curves), the liquid equilibrates to a steady-state value $\phi_{L}(T)$ within <1 ps. The initial liquid achieves a metastable equilibrium enthalpy prior to any phase changes. This equilibrium value of enthalpy remains stationery up to 100–300 ps prior to glass nucleation. For the glass phases formed at 800 and 850 K (red and green curves in Figure 2a), the glass equilibrates on a time scale of 10s of ps. At both temperatures, a well-defined stationery steady-state value of $\phi_{G}(T)$ is established at 2 ns. We take this value to be the metastable equilibrium value of $\phi_{G}(T)$ at the respective T. To validate the assumption of equilibrium, we compare the final

https://dx.doi.org/10.1021/acs.jpclett.9b03699
J. Phys. Chem. Lett. 2020, 11, 632–645

value for each glass (e.g., 11 glasses for 850 K at time 2 ns) to that obtained in the extended MD runs for same glass at 10 ns. The differences are comparable to the noise level of ~3 meV/atom.

We compiled a list of metastable equilibrium values for $\phi_G(T)$ from 750 up to 875 K. To obtain data above 875 K, the glasses that nucleated below 900 K were heated to higher temperatures, held isothermally, and allowed to configurationally equilibrate without crystallizing. The reheating results are provided in Figure S4, SI. Combining this data, we established metastable equilibrium values of $\phi_G(T)$ for temperatures ranging from 750 up to 1100 K. Above 1100 K, the glass phase melts (as described below). Combining results for $\phi_L(T)$ and $\phi_G(T)$, we constructed the metastable equilibrium curve for $\phi_\chi(T) = h_\chi(T, P = 0)$ for the L- and G-phases. Similarly, an enthalpy vs T diagram was constructed for a single crystal of Ag assumed to have zero configurational enthalpy, i.e., $\phi_X(T)$ contains only the vibrational contributions. This amounts to ignoring defects in the single crystal. In fact, few defects are observed in the simulations of the single crystal up to temperatures approaching its melting point, T_{GX}. The $h_\chi(T, P = 0)$ plots for the L-, G-, and X-phases are shown in Figure 5A, where the data are fitted using eq 1. For the single crystal (X), we obtain

$$\phi_X(T) = -2855.9\ \text{mV/atom} + 0.1255T + 2.222 \times 10^{-5}T^2 \quad (2a)$$

where the units for specific enthalpy are meV/atom. For single-crystal fcc Ag, the anharmonic term has an experimental value of $\sim 2 \times 10^{-5}$ (meV/atom·K^2) as estimated from the thermal expansion coefficient and bulk modulus of fcc Ag.[33] Our MD model for fcc Ag gives good agreement with experiment.

Assuming that the metastable liquid from 750 K to high temperature (~1500 K) is at its high-temperature limit with a fixed configurational enthalpy, our fit yields

$$\phi_L(T) = -2761.8\ \text{mV/atom} + 0.1255T + 4.205 \times 10^{-5}T^2 \quad (2b)$$

The assumption that the liquid is at the high-temperature limit is justified by demonstrating that the results give a consistent description of the liquid/crystal phase equilibria. Justification is further provided by the excellent quality of the fits, with a correlation of 99.80% for variance of the fit versus that of the liquid data. To include the T dependence of the liquid configurational enthalpy requires a model. For instance, a traditional model with a Gaussian distribution of inherent states gives a T^{-1} term in addition to the constant term that represents the high-temperature limit. The quality of our fits suggests that such a term must be small over the temperature range where the fitting is carried out. Indeed, there is no argument to suggest that the traditional T^{-1} is an appropriate model. Using the high-temperature approximation, we find that the liquid has significantly higher $\phi^C{}_L(T)$ than the crystal over the range of temperatures of interest (750−1500 K). The liquid also exhibits a greater anharmonicity coefficient by a factor of ~1.9, as might be expected.

For the glass, we once again ignore the T dependence of $\phi^C{}_G(T)$. This is justified if we obtain a consistent description of the heat of crystallization of the glass and heat of the L−G transition over the relevant range of temperature. It is further justified by the excellent quality of the fit to the glass data (a correlation of 99.8% of the variance accounted for). Neglecting configurational contributions to the T dependence of the glass enthalpy is thus reasonable, at least over the temperature range above 700 K. Fitting to the glass yields

$$\phi_G(T) = -2828.3\ \text{mV/atom} + 0.1255T + 3.102 \times 10^{-5}T^2 \quad (2c)$$

The glass data in Figure 5A are from isothermal MD runs and from subsequent MD runs where the metastable glass was heated to higher temperatures (up to 1100 K). At 1125 K and above, the glass was observed to reversibly melt back to an equilibrium liquid. This remelting essentially establishes that the L−G transition is reversible, albeit with a hysteresis effect evidenced by undercooling behavior of the liquid.

The fitted enthalpy curves shown in Figure 5A are assumed to be metastable equilibrium state functions for the L-, G-, and X-phases. As such, the principles of thermodynamics apply, and other thermodynamic state functions such as specific heat, entropy, free energy, etc. may be directly computed from the fits. The entropy of each phase is obtained by integration of dh/T. The integration constant must be determined independently for each phase. The single crystal is a natural choice for a thermodynamic reference state. At its melting point, the entropy of fusion determines the liquid entropy. We use the entropy of the crystal at room temperature as a reference state and fix $s_X(T = 300\ \text{K}, P = 0) = 0$. Room temperature is chosen to avoid quantum effects on vibrational modes when compared with experimental data because the MD simulations are classical. The heat of fusion of single-crystal fcc Ag from MD is 124.9 meV/atom at a melting point of 1250 K. The entropy of fusion is thus 9.639 J/mol·K, of which roughly 2/3 (6.328 J/mol·K) is configurational with the balance vibrational, according to our fits. The entropy of fusion fixes the integration constant for the liquid (relative to the crystal), giving the entropy curves in Figure 5B for the L- and X-phases.

Turning to the glass, the integration constant for the entropy can be fixed by requiring the entropy change upon melting the glass to the liquid at 1125 K agree with that obtained in the coexistence simulation described below. Alternatively, we could force agreement with the heat release observed when the glass nucleates from the liquid at a lower temperature. Using the former method, we obtain the final L, G and X entropy curves in Figure 5B. Because the specific Gibbs free energy (at $P = 0$) is given by $g = h - Ts$, we can also obtain the specific free energy curves for the L-, G-, and X-phases, as shown in Figure 5C. Because the isothermal simulations are done at $P = 0$, the equilibrium or metastable equilibrium volumes of the MD cell are available at each T. The molar volumes data, $v(T)$, for the three phases are shown in Figure 5D.

We now have a rather complete set of approximate thermodynamic state functions for the L-, G-, and X-phases at zero pressure. The results are approximate because we have treated the configurational enthalpy of the phases as an additive constant to the vibrational terms. This assumption is expected to be reasonable over the range of temperatures where the data are available for each phase (i.e., 750−1500 K for the liquid, 750−1125 K for glass).

Returning to the question of the glass structure and how it differs from that of the liquid, we developed a method to reveal how configurational enthalpy is spatially distributed within the system. The time scale for vibrational motion is in the subps range, whereas configurational changes occur over much longer time scales (10 ps−1 ns). To separate the configurational contribution, we do ergodic time averaging of the PE of each

https://dx.doi.org/10.1021/acs.jpclett.9b03699
J. Phys. Chem. Lett. 2020, 11, 632−645

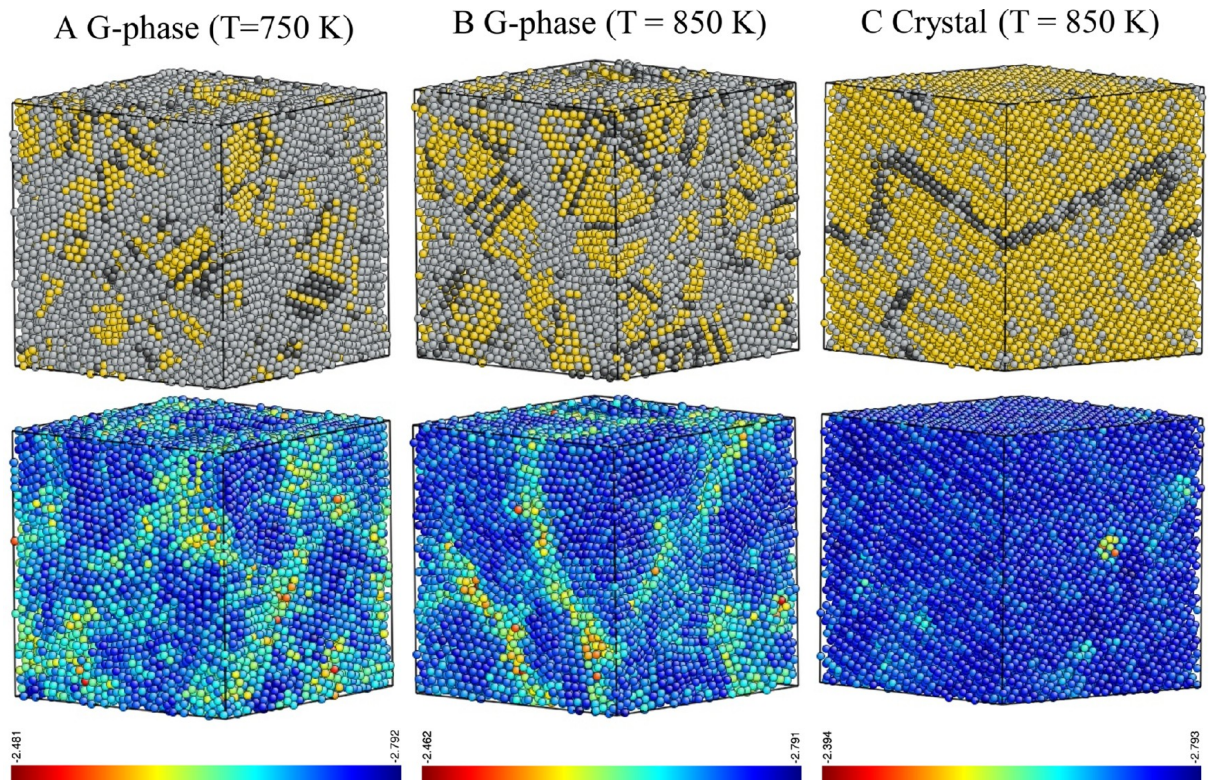

Figure 6. (A–C) Atomic PE density map and local atomic structures of the final glass state at 2 ns and (A) 750 and (B) 850 K; (C) atomic PE density map and local atomic structures of the crystal at 850 K. The fcc, hcp, and other atoms are represented by the yellow, black, and gray balls, respectively. Notice that the low PE ordered regions are isolated and surrounded by liquid-like regions. Further, the ordered regions, while predominantly fcc, also contain many stacking faults (layers of hcp atoms).

atom over 1–2 ps. This time scale is 10^3 times greater than the MD time step (10^{-15} s). Essentially, we perform an ergodic average over vibrational motion. The resulting PE for each atom is averaged over many periods of vibrational motion. Provided that the averaging is done on a time scale sufficiently shorter than the configurational relaxation time, this eliminates vibrational noise to reveal only the atomic variations in the configurational term. Figure 6A,B shows spatial maps of such a vibrationally averaged PE for each atom throughout the final glass structure following 2 ns of MD time at 750 and 850 K. These spatial maps yield the atomic variations in $\phi^{C}{}_{G}(T)$ to reveal a distinct heterogeneous structure within the glass phase. For comparison, the same map for the crystallized structure at 850 K is shown in Figure 6C. An instructive movie showing the temporal development of this structure as the glass forms from the liquid is included in the SI.

To correlate these PE density maps with local atomic structures, we used the HA analysis to identify the fcc, hcp, and other atoms, as shown in Figure 6A–C. Several features of the glass phase are notable. The heterogeneous structure in Figure 6A consists of ordered regions with low $\phi^{C}{}_{G}(T)$ (dark blue) and disordered regions of higher $\phi^{C}{}_{G}(T)$ (yellow/green). The ordered regions possess substantial fcc short-range order (with a relatively high density of octahedral interstitial sites) and resemble close-packed nanocrystals but with visible curvature in the atomic planes. This curvature suggests that these regions are either under substantial elastic stress or that they contain "plastic" defects that serve to accommodate the curvature. These "solid-like" ordered regions are topologically isolated and surrounded by disordered "liquid-like" regions with consistently higher $\phi^{C}{}_{G}(T)$. Our analysis reveals that the liquid-like disordered regions contain diverse atomic environments and a small degree of icosahedral order and generally are more polytetrahedrally packed than the ordered regions. The metastability of this heterogeneous structure over 2–10 ns implies that at both 750 and 850 K the glass contains no supercritical fcc nuclei. The glass structure is a mixture of fcc-like core regions embedded in a surrounding liquid-like disordered medium. The scale of the nanostructure appears to depend on temperature, with the 850 K glass exhibiting a noticeably coarser heterogeneous nanostructure. We refer to the length scale of heterogeneity as $\Lambda(T)$. To investigate the glass stability and the variation of $\Lambda(T)$ with T, we heated the G-phases nucleated at low temperature (below 900 K) to higher temperatures and allowed them to equilibrate isothermally. Upon heating to 950–1200 K, the metastability of the glass with respect to crystallization became very robust. Crystallization was not observed in any of the coexistence MD simulations.

To further confirm the metastability of the G-phase, we computed the Gibbs free energy (G_f) of each atom in the G-phase at 800 K using the two-phase thermodynamics (2PT) model.[34] In 2PT, the thermodynamic properties, such as entropy (S) and Helmholtz free energy (F), are derived from the vibrational density of states obtained from the Fourier transform of the velocity autocorrelation function along a 20 ps trajectory. Thus, the Gibbs free energy is $G_f = F + PV$, where P is

https://dx.doi.org/10.1021/acs.jpclett.9b03699
J. Phys. Chem. Lett. 2020, 11, 632–645

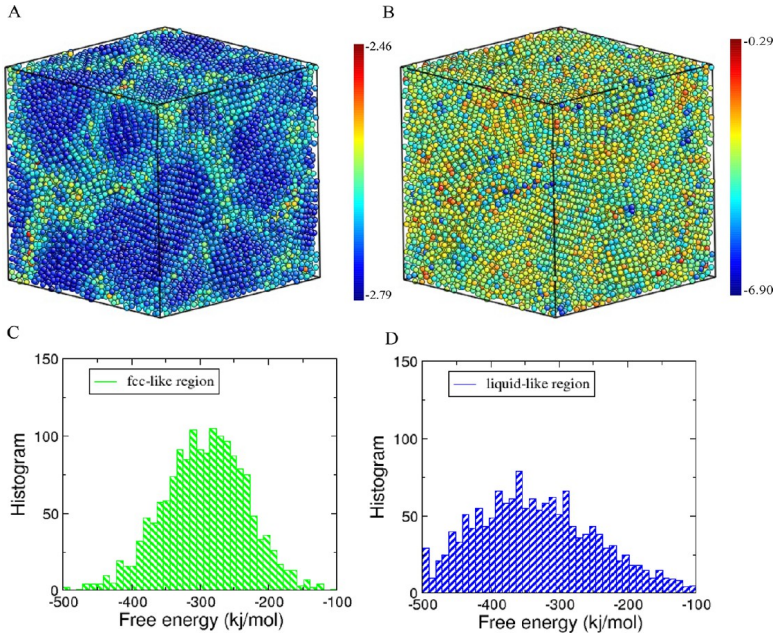

Figure 7. (A,B) Atomic PE density map (A) and free energy map (B) of the final glass state at 2 ns and 800 K. The unit of energy in the legend is eV. (C,D) Free energy distribution of a fcc-like core region (C) and liquid-like region (D).

the atomic pressure and V is the atomic volume. The PE density map and G_f map are displayed in Figure 7A,B, respectively. Although the fcc-like regions have a lower PE than the liquid-like regions, the G_f is essentially constant between these regions. This suggests that the G-phase structure is in thermal equilibrium, validating the stability of the G-phase. We also examined the G_f distribution in the fcc-like core region and liquid-like disordered region, as shown in Figure 7C,D. The liquid-like region shows a broader distribution of G_f, suggesting larger fluctuations than the core region, while the average G_f values of these two regions are very similar.

The free energy diagrams of the L-, G-, and X-phases in Figure 5C predict that the metastable G- and L-phases should coexist at a temperature in the neighborhood of 1100 K. To examine coexistence, we prepared a 32 000 atom glass at 850 K, then heated it to various higher temperatures, and allowed equilibration. This glass was then brought into contact with a 32 000 atom liquid system prepared by undercooling from high temperature so that it contained no glass. The two systems were brought into thermal contact at various temperatures to form a 64 000 atom, ~8 nm × 8 nm × 16 nm system that was allowed to evolve under isothermal MD,[35] as shown in Figure 8A. A spatial map of the vibrationally averaged PE of each atom and the total overall average PE $\phi^{C}_{G}(T)$ per atom during the evolution are shown in Figure 8B. Below 1125 K, the initial liquid phase freezes to glass, while above 1125 K, the initial glass melts and the system becomes entirely liquid, as shown in Figure 8C,D. No crystallization is observed during any of these coexistence simulations (2 ns). The crystalline phase must nucleate from either the glass or liquid, but nucleation of the fcc crystal is not expected at the shallow undercoolings (with respect to $T_{X,M}$ = 1250 K) of the coexistence simulations. We conclude that L- and G-phases coexist in metastable equilibrium at $T_{G,M} \approx 1125$ K (Figure 8A), as predicted by the free energy diagram in Figure 5C. This is the melting point $T_{G,M}$ of the G-phase. We see that the L−G interface in Figure 8B becomes quite rough during melting and/or solidification. Because the G-phase is inherently heterogeneous on the length scale Λ, a sharp interface is not expected. During equilibration (melting or solidification) near $T_{G,M}$, Λ monotonically increases to ~4−5 nm. This compares with $\Lambda \approx 2-3$ nm for glasses initially obtained at 750−850 K. This suggests that Λ exhibits an inherent temperature dependence, but it could be that coarsening of the glass structure is occurring.

The melting point of the fcc Ag single-crystal system was determined using similar L−X two-phase simulations to be $T_{X,m} \approx 1250$ K (see Figure S1). This compares favorably with the experimental melting point of fcc Ag (1234 K), providing additional evidence for the accuracy of the EAM force field used in our simulations. At the L−G coexistence temperature, the liquid and glass are both undercooled with respect to the X-phase by only ~125 K. As a result, crystal nucleation rates are evidently very low and not observable on the MD time scale of the coexistence simulations. The two-phase simulations confirm the prediction of a coexistence point, as implied by the free energy diagram of Figure 5C. They further confirm that the L- and G-phases are separate and distinct metastable phases connected by a first-order melting transition.

To understand the underlying physical origin of the glass state and its relationship to the liquid state, we examined the role of long-range elasticity and stress in stabilizing the glass. It is of particular interest to compare the shear rigidity of the L- and G-phases. To validate the EAM potential for Ag, we computed the elastic constants of the single-crystal Ag at room temperature. We obtained C_{11} = 122.1 GPa, C_{12} = 90.9 GPa, and C_{44} = 46.2 GPa, in good agreement with experimental values of C_{11} = 124.0 GPa, C_{12} = 93.7 GPa, and C_{44} = 46.1 GPa,[36] indicating that our EAM force field accurately captures the elastic properties of metallically bonded Ag.

https://dx.doi.org/10.1021/acs.jpclett.9b03699
J. Phys. Chem. Lett. 2020, 11, 632−645

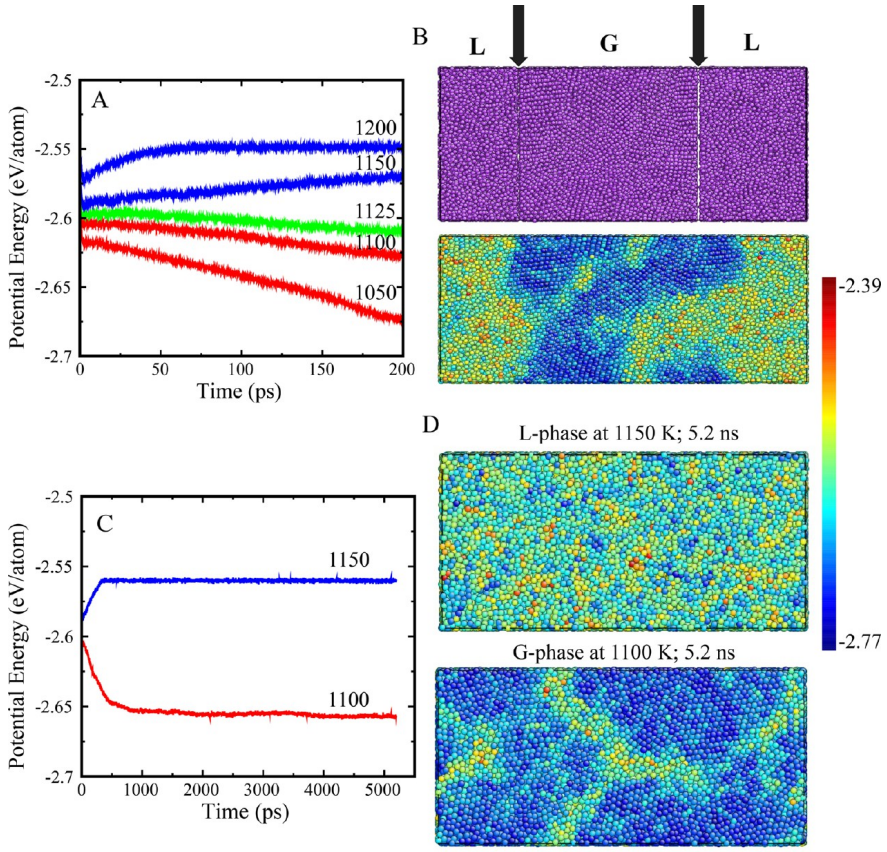

Figure 8. Two-phase L−G simulations to determine the equilibrium $T_{G,M}$: (A) PE evolution of two-phase simulations at various temperatures; (B) two-phase simulation model (0 ps) and PE map (200 ps) at 1125 K; (C) long time simulations at 1100 and 1150 K; (D) PE maps for liquid and crystal phases after long time simulations (5.2 ns).

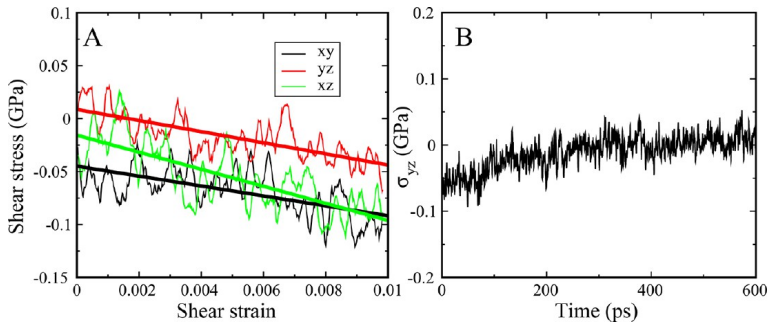

Figure 9. (A) Shear stress−shear strain relationship and (B) stress relaxation. Simulations at T = 1000 K.

In the context of elasticity, it is important to note that both the L- and G-phases are macroscopically isotropic phases. For a macroscopic sample, the thermodynamic properties of both phases are invariant under rotation or translation, with a unique shear modulus μ. The existence of shear rigidity for any macroscopic phase is in fact always conditioned on the existence of a time scale for configurational changes. Even a crystal under applied shear strain, given sufficient time, will relax the induced stress by formation of dislocations or other defects that give rise to configurational rearrangement to yield a plastic response. In the case of crystals, this is generally ignored as the theory of linear elasticity is based on well-defined elastic constants assumed to be thermodynamic state functions. Likewise, it is generally assumed that liquids do not support shear on any practical time scale. A glass is generally described as a viscous liquid with a very high viscosity or relatively long configurational relaxation time. Glasses support shear over long but finite time scales.

To compare the rigidity of the Ag G-phase to that of the L-phase, we carried out simulations at fixed T under a time-dependent applied shear strain to obtain a time-dependent shear modulus. The entire MD cell was subjected to a rhombohedral

https://dx.doi.org/10.1021/acs.jpclett.9b03699
J. Phys. Chem. Lett. 2020, 11, 632−645

affine shear strain at a relatively low strain rate of 0.25 ns^{-1} or 2.5 $\times 10^8$ s^{-1}. Strain was applied in small (0.1%) increments and the stress response of the system determined. Figure 9A shows the stress/strain response of the G-phase at 1000 K (125 K below $T_{G,M}$) to rhombohedral shear applied in the *xy*, *yz*, and *xz* directions.

We observed a linear elastic response. An average value of μ = 6.0 GPa was obtained for the three directions. For the L-phase at 1000 K, we obtained μ < 1 GPa. Given the noise in the stress response, the values of μ obtained were subject to a significant error of order ±1 GPa. Statistically, the μ for the L-phase was effectively zero within the errors involved, while the G-phase exhibited an unambiguous shear modulus at the applied strain rate. To determine the shear stress relaxation time for the glass, a total strain of 1% was imposed and then held fixed while the stress was allowed to relax under the applied strain, as shown in Figure 9B. We observed a stress relaxation time for the G-phase during glass formation at lower temperatures. Using a simple Maxwell model, an estimate of the viscosity of the glass was $\eta_G(1000\ K) = \mu \times \tau \approx 1.8$ Pa·s. This is far higher (by 3 orders of magnitude) than the known experimental viscosity of liquid Ag near its melting point (1240 K), reported to be $\sim 4 \times 10^{-3}$ Pa·s. On the basis of this analysis, the viscosity of the Ag G-phase at 1000 K is 2−3 orders of magnitude greater than that of liquid Ag. Thus, the L−G transition is accompanied by a discontinuous jump in viscosity of the liquid. That is, our Ag G-phase is a relatively viscous liquid with a shear modulus that persists over time scales comparable to its metastability. This is an extremely important observation because it implies that configurational rearrangements in the glass phase are subject to long-range elastic constraints arising from elastic compatibility requirements. Such constraints reduce the configurational entropy of the glass relative to that of the liquid, consistent with the observed entropy drop at the L−G transition. It is notable that hysteresis effects in the undercooled liquid viscosity of well-known bulk metallic glass-forming alloys have been reported, showing jumps of 2−3 orders of magnitude as the hysteresis loop is traversed.[13] The same liquids exhibit hysteresis effects in the molar volume of the liquid versus T.[15] Both observations bear remarkable resemblance to the behavior of the L- and G-phases of Ag presented here.

The first-order L−G transition reported in this work is a transformation from one macroscopically isotropic metastable phase (the undercooled L-phase) to another isotropic metastable solid-like G-phase. We refer to the G-phase as a glass, although its viscosity, $\eta(1000\ K) \approx 2$ Pa·s, is far lower than that of a laboratory glass at its kinetic glass transition, i.e., $\eta \approx 10^{12}$ Pa·s. Laboratory glasses are kinetically stabilized in real time against crystallization as the temperature is lowered toward the conventional T_g. The G-phase in Ag exhibits enhanced metastability with respect to crystallization near its melting point, $T_{G,M}$. The concept of glass metastability is meaningful only if defined with respect to the relaxation time for its configurational degrees of freedom. To achieve metastable equilibrium, the L- or G-phases must explore all noncrystalline configurations available at a given T before crystallization intervenes. In a bulk laboratory metallic glass near its T_g, metastability is quantified by comparing the configurational (Maxwell) relaxation time to the crystallization time. The ratio of the latter to the former quantifies the extent to which the glass equilibrates and thereby determines the applicability of thermodynamics. For laboratory glasses near T_g, crystallization typically occurs over minutes, hours, or days,[20] whereas the Maxwell relaxation time (at T_g) is typically 10−100 s. Thus, the ratio is typically $\sim 10^2$−10^5. The configurational (Maxwell) relaxation time of the Ag G-phase ranges from 10 to 100s of ps depending on temperature, while we found its crystallization time to depend on system size. For the 256 000 atom case where finite size-induced crystallization (the MD cell-spanning mechanism) is suppressed, our results show that crystallization is essentially absent on practical MD time scales (~50 ns) at all temperatures of 750 K or higher. Thus, the ratio of the crystallization time to the Maxwell relaxation time is at least of order 10^3, similar to typical laboratory metallic glasses near T_g. In this view, the degree of metastability is comparable for the simulation and laboratory cases. These arguments emphasize that metastability is a relative concept.

The L-phase is homogeneous on the atomic scale, while the G-phase displays a distinct heterogeneous topological structure with a characteristic length scale Λ, typically several nanometers. The G-phase contains isolated ordered regions with local fcc-like short-range order, having a lower (than average) PE per atom. The HA analysis shows that these regions contain clusters of atoms with fcc- or hcp-type atomic environments. These regions exhibit strongly curved atomic planes, point defect clusters, stacking faults, and dislocation defects. They are isolated topologically, being surrounded by liquid-like regions. This indicates that they are not equilibrium crystals. The ordered regions are surrounded by a continuous matrix of disordered liquid-like regions having noncrystalline atomic structure, high configurational enthalpy, and greater polytetrahedral short-range order. Owing to this heterogeneous structure, the ordered regions are incoherent with neighboring order regions. Therefore, there is no long-range order on length scales exceeding Λ ~ 2 nm, the size of these regions. It is this feature that leads us to conclude that the G-phase is non-crystalline as opposed to a crystalline state.

The L−G transition is first-order and occurs by nucleation of the G-phase from the undercooled L-phase at a significant degree of undercooling. For example, the G-phase nucleated from the liquid at 750−850 K is undercooled by 275−375 K with respect to its melting temperature $T_{G,M}$ = 1125 K. The freezing/melting transition of the G-phase is reversible, albeit with significant hysteresis. The glassy G-phase coexists in metastable equilibrium with the liquid L-phase at its melting point $T_{G,M}$ = 1125K. The G-phase is further distinguished from the L-phase by the emergence of elastic rigidity with a finite persistent shear modulus, μ(T). We suggest that the discontinuous emergence of global rigidity in the G-phase results in long-range elastic interactions between spatially separated local configurational excitations. In metallic glasses, these configurational excitations are known to have a string-like character[37,38] and involve localized cooperative rearrangements of roughly 10−20 atoms.[39] This cooperative atomic rearrangement gives rise to a characteristic plastic strain of the rearranging core atomic cluster. As shown by Eshelby,[40] a localized plastic strain within this core induces a long-range elastic stress field in the surrounding elastic medium. This stress field in turn perturbs energy levels of other spatially separated string defects, resulting in "defect−defect" interactions that are of the long-range power-law type, extending far beyond the range of local interactions between atoms. The first-order character of the observed L−G transition in Ag is thus likely related to the emergence of these long-range interactions.

https://dx.doi.org/10.1021/acs.jpclett.9b03699
J. Phys. Chem. Lett. 2020, 11, 632−645

■ ASSOCIATED CONTENT

Supporting Information

The Supporting Information is available free of charge at https://pubs.acs.org/doi/10.1021/acs.jpclett.9b03699.

Simulation details, HA index of the G-phase and liquid, melting temperature of the crystal Ag from two-phase simulation, extended RDF and structure factor analysis on X-, L-, and G-phases, statistics simulations at various temperatures, and Ag glass remelting (PDF)

Movie showing the glass nucleation at 750 K using the potential energy density map (AVI)

■ AUTHOR INFORMATION

Corresponding Authors

Qi An − *University of Nevada—Reno, Reno, Nevada;* orcid.org/0000-0003-4838-6232; Email: qia@unr.edu

William L. Johnson − *California Institute of Technology, Pasadena, California*; Email: wlj@caltech.edu

William A. Goddard, III − *California Institute of Technology, Pasadena, California;* orcid.org/0000-0003-0097-5716; Email: wag@caltech.edu

Other Authors

Konrad Samwer − *University of Goettingen, Goettingen, Germany*

Sydney L. Corona − *California Institute of Technology, Pasadena, California*

Complete contact information is available at: https://pubs.acs.org/10.1021/acs.jpclett.9b03699

Notes

The authors declare no competing financial interest.

■ ACKNOWLEDGMENTS

Q.A. is supported by the U.S. Nuclear Regulatory Commission (NRC) under Grant No. NRC-HQ-84-15-G-0028. W.L.J and S.C. are supported by NSF Grant Award Number DMR 1710744. K.S. is supported by the DFG, Grant Sa337/10. W.A.G. thanks ONR (N00014-19-1-2081) for support.

■ REFERENCES

(1) Goldstein, M. Viscous liquids and glass transition − a potential energy barrier picture. *J. Chem. Phys.* **1969**, *51*, 3728−3739.

(2) Stillinger, F. H.; Debenedetti, P. G. Glass transition thermodynamics and kinetics. *Annu. Rev. Condens. Matter Phys.* **2013**, *4*, 263−285.

(3) Debenedetti, P. G.; Stillinger, F. H. Supercooled liquids and the glass transition. *Nature* **2001**, *410*, 259−267.

(4) Sciortino, F.; Kob, W.; Tartaglia, P. Inherent structure entropy of supercooled liquids. *Phys. Rev. Lett.* **1999**, *83*, 3214−3217.

(5) Martinez, L. M.; Angell, C. A. A thermodynamic connection to the fragility of glass-forming liquids. *Nature* **2001**, *410*, 663−667.

(6) Wales, D. J. *Energy landscapes: applications to clusters, biomolecules, and glasses*; Cambridge University Press: Cambridge, U.K., 2004.

(7) Mishima, O.; Suzuki, Y. Propagation of the polyamorphic transition of ice and the liquid-liquid critical point. *Nature* **2002**, *419*, 599−603.

(8) Zhu, M.; Wang, J. Q.; Perepezko, J. H.; Yu, L. Possible existence of two amorphous phases of d-mannitol related by a first order phase transition. *J. Chem. Phys.* **2015**, *142*, 244504.

(9) Cohen, I.; Ha, A.; Zhao, X.; Lee, M.; Fischer, T.; Strouse, J. J.; Kivelson, D. A low-temperature amorphous phase in a fragile glass-forming substance. *J. Phys. Chem.* **1996**, *100*, 8518−8526.

(10) McMillan, P. F.; Wilson, M.; Daisenberger, D.; Machon, D. A density-driven phase transition between semiconducting and metallic polyamorphs of silicon. *Nat. Mater.* **2005**, *4*, 680−684.

(11) Katayama, Y.; Tsuji, K. X-ray structural studies on elemental liquids under high pressures. *J. Phys.: Condens. Matter* **2003**, *15*, 6085−6103.

(12) Monaco, G.; Falconi, S.; Crichton, W. A.; Mezouar, M. Nature of the first-order phase transition in fluid phosphorus at high temperature and pressure. *Phys. Rev. Lett.* **2003**, *90*, 255701.

(13) Way, C.; Wadhwa, P.; Busch, R. The influence of shear rate and temperature on the viscosity and fragility of Zr-Ti-Cu-Ni-Be metallic glass-forming liquid. *Acta Mater.* **2007**, *55*, 2977−2983.

(14) Sheng, H. W.; Liu, H. Z.; Cheng, Y. Q.; Wen, J.; Lee, P. L.; Luo, W. K.; Shastri, S. D.; Ma, E. Polyamorphism in a metallic glass. *Nat. Mater.* **2007**, *6*, 192−197.

(15) Li, J. J. Z.; Rhim, W. K.; Kim, C. P.; Samwer, K.; Johnson, W. L. Evidence of a liquid-liquid phase transition in metallic fluids by electrostatic levitation. *Acta Mater.* **2011**, *59*, 2166−2171.

(16) Turnbull, D. Metastable structures in metallurgy. *Metall. Trans. A* **1981**, *12* (5), 695−708.

(17) Willnecker, R.; Herlach, D. M.; Feuerbacher, B. Evidence of nonequilibrium processes in rapid solidification of undercooled metals. *Phys. Rev. Lett.* **1989**, *62*, 2707−2710.

(18) Schenk, T.; Holland-Moritz, D.; Simonet, V.; Bellissent, R.; Herlach, D. M. Icosahedral short-range order in deeply undercooled metallic melts. *Phys. Rev. Lett.* **2002**, *89*, No. 075507.

(19) Holland-Moritz, D.; Schenk, T.; Bellissent, R.; Simonet, V.; Funakoshi, K.; Merino, J. M.; Buslaps, T.; Reutzel, S. Short-range order in undercooled Co melts. *J. Non-Cryst. Solids* **2002**, *312*−*314*, 47−51.

(20) Johnson, W. L.; Na, J. H.; Demetriou, M. D. Quantifying the origin of metallic glass formation. *Nat. Commun.* **2016**, *7*, 10313.

(21) Buckel, W.; Hilsch, R. Influence of condensation at low temperatures on the electrical resistance and superconductivity for different metals. *Eur. Phys. J. A* **1954**, *138*, 109−120.

(22) Coriell, S. R.; Turnbull, D. Relative roles of heat transport and interface rearrangement rates in the rapid growth of crystals in undercooled melts. *Acta Metall.* **1982**, *30*, 2135−2139.

(23) Zhong, L.; Wang, J.; Sheng, H.; Zhang, Z.; Mao, S. X. Formation of monatomic metallic glasses through ultrafast liquid quenching. *Nature* **2014**, *512*, 177−180.

(24) An, Q.; Luo, S.-N.; Goddard, W. A.; Han, W. Z.; Arman, B.; Johnson, W. L. Synthesis of single-component metallic glasses by thermal spray of nanodroplets on amorphous substrates. *Appl. Phys. Lett.* **2012**, *100*, No. 041909.

(25) Powell, G. L. F. The undercooling of silver. *J. Austr. Inst. Metall.* **1965**, *12*, 223−230.

(26) Muskhelishvili, N. I. *Some basic problems of the mathematical theory of elasticity*; Springer: Dordrecht, The Netherlands, 2010.

(27) Williams, P. L.; Mishin, Y.; Hamilton, J. C. An embedded-atom potential for the Cu−Ag system. *Modell. Simul. Mater. Sci. Eng.* **2006**, *14*, 817−833.

(28) Plimpton, S. Fast parallel algorithms for short-range molecular dynamics. *J. Comput. Phys.* **1995**, *117*, 1−19.

(29) Schawe, J. E. K.; Löffler, J. F. Existence of multiple critical cooling rates which generate different types of monolithic metallic glass. *Nat. Commun.* **2019**, *10*, 1337.

(30) Turnbull, D. Formation of crystal nuclei in liquid metals. *J. Appl. Phys.* **1950**, *21*, 1022−1028.

(31) Perepezko, J. H. Nucleation in undercooled liquids. *Mater. Sci. Eng.* **1984**, *65*, 125−135.

(32) Honeycutt, J. D.; Andersen, H. C. Molecular dynamics study of melting and freezing of small lennard-jones clusters. *J. Phys. Chem.* **1987**, *91*, 4950−4963.

(33) Brillo, J.; Egry, I.; Ho, I. Density and thermal expansion of liquid Ag−Cu and Ag−Au alloys. *Int. J. Thermophys.* **2006**, *27*, 494−506.

(34) Lin, S. T.; Blanco, M.; Goddard, W. A., III The two-phase model for calculating thermodynamic properties of liquids from molecular dynamics: validation for the phase diagram of lennard-jones fluids. *J. Chem. Phys.* **2003**, *119*, 11792−11805.
(35) An, Q.; Zheng, L. Q.; Fu, R. S.; Ni, S. D.; Luo, S. N. Solid−liquid transitions of sodium chloride at high pressures. *J. Chem. Phys.* **2006**, *125*, 154510.
(36) Neighbours, J. R.; Alers, G. A. Elastic constants of silver and gold. *Phys. Rev.* **1958**, *111*, 707−712.
(37) Stevenson, J. D.; Schmalian, J.; Wolynes, P. G. The shapes of cooperatively rearranging regions in glass-forming liquids. *Nat. Phys.* **2006**, *2*, 268−274.
(38) Yu, H. B.; Wang, W. H.; Bai, H. Y.; Samwer, K. The beta-relaxation in metallic glasses. *Natl. Sci. Rev.* **2014**, *1*, 429−461.
(39) Sheng, H. W.; Ma, E.; Kramer, M. J. Relating dynamic properties to atomic structure in metallic glasses. *JOM* **2012**, *64*, 856−881.
(40) Eshelby, J. D. The determination of the elastic field of an ellipsoidal inclusion, and related problems. *Proc. Royal Soc.* **1957**, *241*, 376−396.

https://dx.doi.org/10.1021/acs.jpclett.9b03699
J. Phys. Chem. Lett. 2020, 11, 632−645